Stability of stationary gap solitary waves at periodically modulated surfaces

J. Schöllmann and R. Scheibenzuber
Institut für Theoretische Physik, Universität Regensburg, D-93040 Regensburg, Germany

A. S. Kovalev
Institute for Low Temperature Physics and Engineering, Ukrainian Academy of Sciences, Kharkov 310164, Ukraine

A. P. Mayer*
Max-Planck-Institut für Physik komplexer Systeme, D-01187 Dresden, Germany

A. A. Maradudin
Department of Physics and Institute for Surface and Interface Science, University of California, Irvine, California 92697
(Received 1 June 1998)

Nonlinear optical waveguides with periodically modulated surfaces or interfaces can support stationary localized waves, often called gap solitons, with frequencies lying in the stop gaps of the spectrum of linear excitations. They are solutions of evolution equations that have been derived for instantaneous Kerr-type, thermal (diffusive) as well as instantaneous resonant and nonresonant second-order nonlinearity. A numerical linear stability analysis is carried out for some examples of these gap solitary wave solutions based on discretization of the spatial coordinate. In addition to numerical instabilities, which are a consequence of discretization and which pose a problem to numerical integration schemes, weak physical instabilities have been found, which correspond to radiation away from the solitary wave. The growth rates are strongly dependent on the boundary conditions imposed at the edges of the spatial domain. Growth rates and radiation frequencies have also been computed for an infinite spatial domain. The influence of the diffusion length on the instability has been investigated. [S1063-651X(99)05104-1]

PACS number(s): 42.65.Tg, 42.81.Dp, 42.70.Qs, 42.65.Sf

I. INTRODUCTION

Nonlinear localized excitations with frequencies in the stop gaps of the frequency spectrum of linear excitations of a periodic system have been observed by Chen and Mills [1] in numerical transmission experiments of light through layered media with third-order nonlinearity and have been termed gap solitons. Subsequently, they have been analyzed theoretically [2–6]. Since then, such nonlinear excitations have been found in several periodic systems that exhibit stop gaps in their linear excitation spectra, mainly in connection with transmission through nonlinear periodic media in different areas of physics (see, e.g., [7,8]). Research on gap solitons has gained new momentum since they have been verified experimentally in a Bragg grating fiber [9]. The role of gap solitons has also been discussed in transmission through periodically corrugated silicon-on-insulator (SOI) waveguides [10–12]. While in the earlier works an instantaneous third-order nonlinearity of the Kerr type had been considered, the nonlinearity in the SOI Bragg gratings is of a diffusive type through coupling of the light to the density of free carriers and to the electronic and lattice temperatures in the semiconductor [13,14]. In the stationary case, this leads to an effective nonlocal third-order nonlinearity, as will be shown below. Periodic systems with second-order nonlinearity have also been shown to give rise to gap solitary waves [15–23]. When the frequency of the second harmonic of the fundamental mode with wave vector at the edges of the Brillouin zone is far from resonance with a waveguide mode, the same evolution equations are obtained as had been derived for the case of Kerr nonlinearity, for which the Mills-Trullinger solitary solutions were found [2,6] (we shall call them the MT equations in the following) with an effective third-order nonlinearity. Inspired by earlier work on nonlinear waveguides without periodic modulation [24], the interesting situation of a (near) resonance of the second harmonic of the fundamental mode at Brillouin zone boundaries with another waveguide mode has been studied [17–23], and solitary wave solutions have been found numerically and, for special choices of the parameters, analytically. For this system, multistability had been studied on the basis of the same evolution equations [25] as used for the determination of solitary waves.

While a variety of gap soliton solutions have been found, little is known about their stability. Apart from very recent work on solitary wave solutions of the MT equations [26], which makes use of the fact that these equations are integrable in the limit of the massive Thirring model [27,28], information on the stability of gap solitary waves has mostly been drawn from numerical simulations. However, it is argued in this paper that simulations do not always give the right answer concerning the stability of gap solitary waves due to the special type of instability occurring in these systems and because of additional numerical instabilities generated by discretization of the spatial coordinate which is a feature of all common numerical methods used in the inte-

*On leave from the Institut für Theoretische Physik, Universität Regensburg, D-93040 Regensburg, Germany.

 ©1999 The American Physical Society

gration of nonlinear evolution equations in nonlinear optics. We therefore carry out a linear stability analysis and diagonalize the resulting non-Hermitian linear operator by discretizing the spatial coordinate. In this way, we identify physical and purely numerical instabilities.

The term gap solitary wave is used here for spatially localized solutions of evolution equations with nonlinearity balancing the effect of linear coupling through the grating between the forward and backward propagating guided waves with wave vectors at the Brillouin zone boundary. Sometimes, the term gap soliton is also used for situations where nonlinearity is a small perturbation compared to the effects of the periodicity of the grating. In this regime, solitary waves are described by the nonlinear Schrödinger (NLS) equation in the case of third-order nonlinearity and by the Karamzin-Sukhorukov (KS) equations in the case of second-order nonlinearity with the second harmonic of the fundamental waveguide mode in (quasi) resonance with another waveguide mode. The stability properties of the solitary wave solutions of these evolution equations are well known [29,30]. These equations also follow from the evolution equations considered here in the limit of small intensities, and one may therefore expect that the stability behavior of gap solitary waves approaches that of the soliton solutions of the NLS and solitary wave solutions of the KS equations in these limits.

Throughout this paper, we have restricted our considerations to stationary gap solitary waves only.

In the following section, we briefly review the evolution equations that have been derived for the different types of nonlinearity and comment on some aspects that do not seem to have been appreciated in earlier works. We consider three different systems which all find realizations in slab waveguide geometries with periodically modulated surface or interfaces: (1) guided *p*-polarized plasmon polaritons on a substrate with an instantaneous third-order (Kerr-type) nonlinearity, (2) guided *s*-polarized polaritons in a waveguide which is nonlinear due to coupling of the electric field to a diffusive degree of freedom, and (3) guided polariton modes interacting (quasi) resonantly with their second harmonic through instantaneous second-order nonlinearity.

We emphasize that the evolution equations derived for these optical systems also partly apply to other physical contexts like guided acoustic waves, for example.

Section III is devoted to the stability analysis for solitary waves found to exist in these three systems, and the paper ends with a short conclusion.

II. EVOLUTION EQUATIONS FOR GAP SOLITARY WAVES

A. Kerr nonlinearity

In the pioneering work of Mills and Trullinger [2] and most of the later studies on gap solitons, the Kerr type of nonlinearity had been considered. Instead of a superlattice with periodically varying dielectric constant, we choose here as an example system the one described in Ref. [32], i.e., a dielectric medium with Kerr-type nonlinearity covered by a metal film with periodically corrugated surface (Fig. 1). Later, we will generalize the system by allowing for the presence of second-order nonlinearity in the substrate. The corrugation is described by the surface profile function $\zeta(x)=\zeta_0\cos(Gx)$. The dielectric substrate fills the half space $z<0$ and the metal film occupies the region $0<z<d+\zeta(x)$. This system supports *p*-polarized guided polaritons in the linear limit also in the case of a flat metal surface. Using standard multiple-scale techniques (see, e.g., Ref. [33]), the MT equations are readily derived for this system. Writing the electrical field $\vec{E}$ in the form of an asymptotic expansion in powers of a small parameter $\nu \ll 1$:

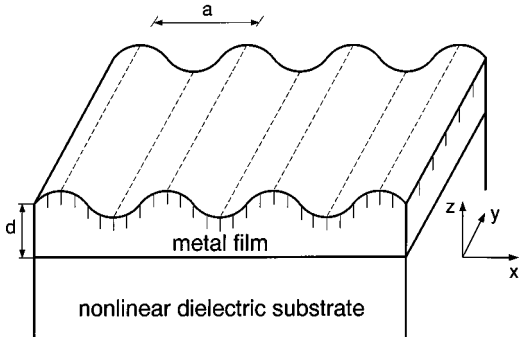

FIG. 1. Geometry of the system considered as an example for a Bragg grating considered in Sec. II A. *d*, average film thickness; $a=2\pi/G$, periodicity of the surface corrugation.

$$\vec{E}=e^{-i\omega_0 t}[\,\nu e^{iGx/2}\vec{E}^{(+)}(z)B_+(X,T)+\nu e^{-iGx/2}\times\vec{E}^{(-)}(z)B_-(X,T)+\nu^3\vec{E}^{(3)}+O(\nu^5)]+\text{c.c.} \quad (2.1)$$

with amplitudes $B_\pm$ depending on stretched coordinates $X=\nu^2 x$ and $T=\nu^2 t$, and scaling $\zeta(x)=\nu^2\tilde{\zeta}(x)=\nu^2\tilde{\zeta}_0\cos(Gx)$, one is led to

$$A_- + i\left(\frac{\partial A_+}{\partial\tau}+\frac{\partial A_+}{\partial\xi}\right)+[N_1|A_+|^2+N_2|A_-|^2]A_+=0, \quad (2.2a)$$

$$A_+ + i\left(\frac{\partial A_-}{\partial\tau}-\frac{\partial A_-}{\partial\xi}\right)+[N_1|A_-|^2+N_2|A_+|^2]A_-=0 \quad (2.2b)$$

after rescaling of the spatial and temporal coordinates $[X\to\xi,\quad T\to\tau,\quad A_\pm(\xi,\tau)=B_\pm(X,T)]$. The fields $\exp[i(\pm Gx/2-\omega_0 t)]\vec{E}^{(\pm)}(z)$ are surface polariton solutions of the linearized wave equation and corresponding boundary conditions for our system with planar interfaces, i.e., in the absence of nonlinearity and periodic corrugation. Details of the derivation are given in Ref. [34], where widths and peak intensities of solitary waves with frequency in the center of the gap in the linear dispersion relation have been evaluated. The results are shown in Table I, the intensity *I* being defined here as $I(X,z)=2|B_\pm(X)\vec{E}_\pm(z)|^2$. For the dielectric constant of the metal film, the simple form $\varepsilon(\omega)=1-\omega_p^2/\omega^2$ has been used with the plasma frequencies ω_p of silver (3.78 eV), aluminum (14.97 eV), and zinc (17.8 eV) [35]. As Kerr coefficients, the data of Ref. [36] have been used for the substrate materials GaAs and InSb. Since the III-V semiconductors allow for second-order nonlinearity in addition to third-order nonlinearity, these data can only be taken as ef-

TABLE I. Spatial extension [full width at half maximum (FWHM)] and maximum intensity I (as defined in the text) of gap solitons for various sets of system parameters. The linear gap width $\Delta\Omega$ is also given. $a=2\pi/G$ is the periodicity of the grating, ζ_0 is its amplitude, and d is the film thickness.

	a (100 nm)	d (100 nm)	ζ_0 (100 nm)	$I_{\max}$ [(V/m)^2]	FWHM (cm)	$\Delta\Omega$ (rad/s)
InSb/Ag	6.0	2.0	0.4	1.81×10^{6}	0.6	3.0×10^{10}
	6.0	2.0	0.2	9.06×10^{5}	1.2	1.5×10^{10}
	6.0	2.0	0.1	4.53×10^{5}	2.39	7.4×10^{9}
	5.5	0.3	0.1	1.31×10^{9}	7.6×10^{-4}	1.9×10^{13}
InSb/Al	6.2	0.35	0.1	1.45×10^{6}	0.76	2.6×10^{10}
	6.2	0.7	0.1	6.95×10^{3}	159.0	1.2×10^{8}
InSb/Zn	6.2	0.3	0.1	1.10×10^{6}	1.0	2.0×10^{10}
	6.2	0.6	0.1	4.79×10^{3}	231.0	8.5×10^{7}
GaAs/Al	1.06	0.65	0.1	2.2×10^{9}	0.7	2.5×10^{10}
	1.06	0.35	0.1	2.9×10^{11}	0.0054	3.3×10^{12}
GaAs/Zn	1.08	1.0	0.1	4.2×10^{5}	3760	5.0×10^{6}
	1.08	0.55	0.1	2.1×10^{9}	0.76	2.5×10^{10}
	1.08	0.3	0.1	2.4×10^{11}	0.0067	2.8×10^{12}

fective Kerr coefficients which are, in principle, geometry dependent. This aspect will be discussed in detail in Sec. II C. For the cases listed in Table I, the maximum of I as a function of the depth coordinate z is reached on the substrate side of the substrate-film interface.

In the limit of small nonlinearity compared to the linear coupling, Eq. (2.2) is easily reduced to a system of two nonlinearly coupled nonlinear Schrödinger equations,

$$i\frac{\partial b_{\pm}}{\partial\tau}\mp\frac{1}{2}\frac{\partial^2 b_{\pm}}{\partial\xi^2}+[(N_1+N_2)|b_{\pm}|^2+2N_1|b_{\mp}|^2]b_{\pm}=0. \tag{2.3}$$

Introducing another expansion parameter $\tilde{\nu}$ and scaling the linear interaction as $\tilde{\nu}^{-1}$, one finds Eq. (2.3) with

$$\begin{pmatrix}A_+(\xi,\tau)\\A_-(\xi,\tau)\end{pmatrix}\approx e^{-i\tau/\tilde{\nu}}\begin{pmatrix}1\\1\end{pmatrix}b_+(\xi,\tau)+e^{i\tau/\tilde{\nu}}\begin{pmatrix}1\\-1\end{pmatrix}b_-(\xi,\tau). \tag{2.4}$$

It should be noted that when deriving the NLS equations (2.3) from the MT equations (2.2), it is assumed that the dispersion of the linear modes at the Brillouin zone boundary is due to the fundamental Fourier component of the grating with wave number G only. If one relaxes this condition, one can still derive the NLS equations (2.3), but the coefficient in front of the second spatial derivative may be influenced by physical dispersion, waveguide dispersion in the absence of the grating, and by higher Fourier components of the grating's profile function in the case of a deep grating.

B. *s*-polarized gap solitary waves in waveguides with diffusive nonlinearity

Recently, transmission of *s*-polarized light has been studied in nonlinear silicon-on-insulator waveguides with periodically corrugated surfaces. The geometry is similar to that of Fig. 1 with the metal film now replaced by a silicon film and the dielectric substrate replaced by a thick SiO_2 layer on a silicon substrate. In these systems, the optical nonlinearity results from free carriers generated by the light intensity. These charge carriers influence the refractive index of the waveguide directly or indirectly via the thermo-optic effect by locally heating the lattice. These effects can be described approximately by three coupled diffusion equations for the carrier concentration, the carrier temperature, and the lattice temperature [13,14], which are in turn coupled to Maxwell's equations.

An important feature of these equations is the presence of diffusion terms which may have a strong influence on the spatial distribution of the intensity in a gap soliton solution. To keep the following calculations as simple as possible while still capturing this important feature, we consider the following model, in which one diffusion equation is coupled to the electromagnetic field in the film:

$$\frac{\partial n}{\partial t}+\frac{n}{\tau_r}-D\Delta n=\alpha|\vec{E}|^2, \tag{2.5}$$

$$\frac{\partial^2}{\partial t^2}\frac{\varepsilon}{c^2}\vec{E}+\vec{\nabla}\times(\vec{\nabla}\times\vec{E})=-\frac{\partial^2}{\partial t^2}K_c n\vec{E}, \tag{2.6}$$

where Δ is the Laplace operator. To keep the notation simple, the dispersion of the dielectric constant has not been indicated explicitly in Eq. (2.6), but will be accounted for in the following. However, we shall neglect all losses to the electromagnetic field for simplicity. The quantity n represents either the carrier concentration, or the lattice or carrier temperature. A generalization to three coupled equations of the type of Eq. (2.5) is straightforward. In addition to the electromagnetic boundary conditions, we require that the component of the gradient of n normal to the boundaries of the silicon film has to vanish at these boundaries.

To the coupled system of partial differential equations (2.5) and (2.6) we may again apply an asymptotic analysis, expanding the electric field as Eq. (2.1) and scaling $n=O(\nu^2)$. Following the asymptotic scheme, we have to solve an inhomogeneous partial differential equation for $n(x,z)$ to second order in the expansion parameter ν and insert its solution into Eq. (2.6). The compatibility conditions for the solvability for $\vec{E}^{(3)}$ then yield the evolution equations (2.2) with coefficients N_1 and N_2 depending on ω_0, G, the relaxation time τ_r, and the diffusion constant D.

For large diffusion constants, the coefficients N_1 and N_2 become equal. While in the above treatment, the variations of the quantity n on long time and long length scales T and X follow those of the intensity of the light, this is not necessarily the case for large diffusivity. In order to account for this effect, we introduce a different scaling of the parameters in Eq. (2.5) by writing it in the form

$$\nu^{-2}\tau_r\frac{\partial n}{\partial t}+n-\nu^{-4}D\tau_r\Delta n=\tau_r\alpha|\vec{E}|^2. \tag{2.7}$$

Expanding $n=\nu^2 n^{(2)}+\nu^3 n^{(3)}+O(\nu^4)$ and inserting this together with Eq. (2.1) into Eq. (2.7), one finds that $n^{(2)}$ is independent of the short scales t, x, and

$$\rho+\tau_R\frac{\partial}{\partial\tau}\rho-\kappa^2\frac{\partial^2}{\partial\xi^2}\rho=[|A_+|^2+|A_-|^2], \tag{2.8}$$

where $\tau\propto T,\xi\propto X,\rho(\xi,\tau)\propto n^{(2)}(X,T)$, and $A_\pm(\xi,\tau)\propto B_\pm(X,T)$. This equation is coupled to the two equations for the field amplitudes,

$$A_\mp+i\left(\frac{\partial A_\pm}{\partial\tau}\pm\frac{\partial A_\pm}{\partial\xi}\right)+S\rho A_\pm=0, \tag{2.9}$$

where $S=\pm1$. In the following, we consider the positive sign only. Equation (2.9) is obtained by inserting Eq. (2.1) and the expansion for n into Eq. (2.6) and applying the usual multiple-scale procedure with $T=\nu^2 t$ and $X=\nu^2 x$. The rescaling leading from $T,X,n^{(2)},B_\pm$ to $\tau,\xi,\rho,A_\pm$ has been made to eliminate constant coefficients from the evolution equations. The remaining parameters are the effective diffusion length κ and relaxation time τ_R. In the limit $\tau_R=0$, the variable ρ is readily eliminated to yield two coupled evolution equations of the form (2.2) with, however, a nonlocal nonlinearity,

$$\begin{aligned}A_\mp(\xi,\tau)+i\left(\frac{\partial}{\partial\tau}\pm\frac{\partial}{\partial\xi}\right)A_\pm(\xi,\tau)\\ +\frac{S}{2\kappa}\int_{-\infty}^{\infty}e^{-|\xi-\xi'|/\kappa}[|A_+(\xi',\tau)|^2\\ +|A_-(\xi',\tau)|^2]d\xi' A_\pm(\xi,\tau)=0.\end{aligned} \tag{2.10}$$

In order to find stationary solutions to Eqs. (2.8) and (2.9) that correspond to the gap solitary waves found by Mills and Trullinger in the limit $\kappa=0$, we start with the ansatz

$$A_+(\xi,\tau)=U(\xi)e^{-i\delta\tau},\quad A_-(\xi,\tau)=U^*(\xi)e^{-i\delta\tau} \tag{2.11}$$

and require ρ to be independent of τ. Furthermore, we impose the condition that the real part of U is an odd function while its imaginary part is an even function of ξ. The diffusion length κ sets here an additional scale for the width of spatially localized solutions. The conservation law

$$U^2+(U^*)^2+2(\rho+\delta)|U|^2+\frac{\kappa^2}{2}\left(\frac{\partial\rho}{\partial X}\right)^2-\frac{1}{2}\rho^2=0 \tag{2.12}$$

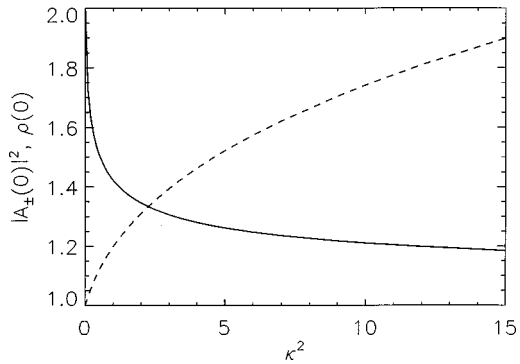

FIG. 2. Maximum values of the field intensity $[|A_\pm(0)|^2$, dashed curve] and of the carrier concentration $[\rho(0)$, solid curve] as a function of the diffusion length κ (arbitrary units) for gap solitary wave solutions of Eqs. (2.8) and (2.9) with frequency in the center of the gap ($\delta=0$).

establishes a relation between the values of ρ and the imaginary part of U at $\xi=0$.

Figure 2 shows the maximum values of the intensity $|A_\pm|^2$ and the variable ρ as a function of the square of the diffusion length κ. As may have been expected, the width of the stationary solitary wave solutions increases with increasing diffusion length. As may be seen from Fig. 3, this is much more the case for the quantity ρ than for the intensity $|A_\pm|^2$ of the electromagnetic field.

We note that in Eqs. (2.8) and (2.9), the charge $\int[|A_+(\xi,\tau)|^2+|A_-(\xi,\tau)|^2]d\xi$ is a conserved quantity, while energy and momentum conservation only hold in the limit $\tau_R=0$.

In addition to the stationary solutions found by Mills and Trullinger, moving solitary solutions have also been found [6] for the two coupled equations (2.2). Analogous solutions of Eqs. (2.8) and (2.9) would be attenuated due to the time derivative occurring in Eq. (2.8), which is not effective in the stationary case.

C. Quadratic nonlinearity in the nonresonant case

In the presence of second-order nonlinearity, the electromagnetic wave with frequency ω_0 generates a second harmonic. We first consider a situation in which this second harmonic is not resonant with a waveguide mode, which

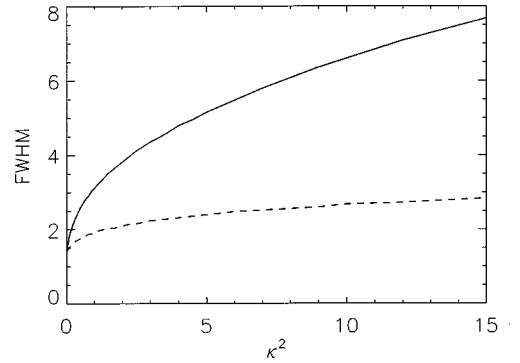

FIG. 3. Full width at half maximum of the field intensity ($|A_\pm|^2$, dashed curve) and of the carrier concentration (ρ, solid curve), associated with a gap solitary wave solution with $\delta=0$, as a function of the diffusion length κ (arbitrary units).

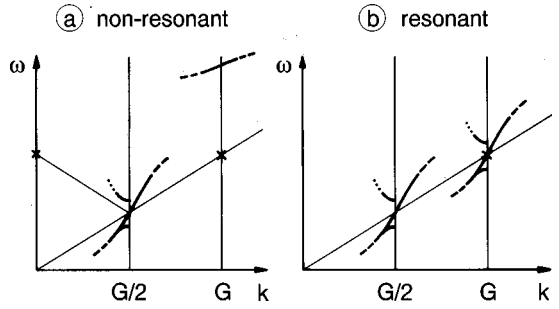

FIG. 4. Nonresonant (left) and resonant (right) interaction of carrier wave components with their second harmonic, schematically. The thick lines represent parts of the dispersion curves of linear guided modes.

situation has also been treated in Ref. [15]. As an example, we choose again the waveguide system of Fig. 1. We assume that there is no waveguide mode with wave vector $\pm G$ and frequency equal or close to $2\omega_0$ in the absence of nonlinearity and periodic modulation.

In this case, which is illustrated schematically in the left part of Fig. 4, the second harmonic can be included in the asymptotic expansion (2.1) by adding to the right-hand side of Eq. (2.1) the term

$$e^{-2i\omega_0 t}[\,\nu^2 e^{iGx}\vec{E}^{(+2,2)}(z)B_+^2(X,T) + \nu^2 e^{-iGx}\vec{E}^{(-2,2)}(z)B_-^2(X,T) + \nu^2\vec{E}^{(0,2)}(z)B_+(X,T)B_-(X,T)+O(\nu^3)]+\text{c.c.} \quad (2.13)$$

The functions $\vec{E}^{(\pm 2,2)}$ and $\vec{E}^{(0,2)}$ are solutions of the field equations to second order in the expansion parameter ν and the corresponding boundary conditions at the planar interfaces and at infinity. These field equations have the form

$$\left\{\varepsilon_L(2\omega_0)\left(\frac{2\omega_0}{c}\right)^2+(1-\delta_{\alpha z})\frac{\partial^2}{\partial z^2}\right\}E_\alpha^{(0,2)} = -\left(\frac{2\omega_0}{c}\right)^2 2\sum_{\beta,\gamma}\chi^{(2)}_{\alpha\beta\gamma}E_\beta^{(+)}E_\gamma^{(-)} \quad (2.14)$$

$$\sum_\beta\left\{\varepsilon_L(2\omega_0)\left(\frac{2\omega_0}{c}\right)^2\delta_{\alpha\beta} + \sum_\gamma \vec{\nabla}_\gamma^{(\pm)}\vec{\nabla}_\gamma^{(\pm)}\delta_{\alpha\beta}-\vec{\nabla}_\alpha^{(\pm)}\vec{\nabla}_\beta^{(\pm)}\right\}E_\beta^{(\pm 2,2)} = -\left(\frac{2\omega_0}{c}\right)^2\sum_{\beta,\gamma}\chi^{(2)}_{\alpha\beta\gamma}E_\beta^{(\pm)}E_\gamma^{(\pm)}. \quad (2.15)$$

Here, $\varepsilon_L(\omega)$ is the linear dielectric function which depends on frequency and on the spatial coordinate z, the $\chi^{(2)}_{\alpha\beta\gamma}$ are the coefficients occurring in the second-order term in the expansion of the polarization with respect to the electric field, and α,β,γ are Cartesian indices. In addition, we have defined $\vec{\nabla}_x^{(\pm)}=\pm iG$, $\vec{\nabla}_y^{(\pm)}=0$, and $\vec{\nabla}_z^{(\pm)}=\partial/\partial z$. The inhomogeneous equations (2.14) and (2.15) can be solved in a straightforward way. The boundary conditions at the interfaces and at $z=\pm\infty$ guarantee the uniqueness of their solutions. In the next step, the solutions of Eqs. (2.14) and (2.15) are inserted into the field equations of order $O(\nu^3)$ in the asymptotic procedure, which are projected on the modal fields $\vec{E}^{(\pm)}(z)$ to obtain again the evolution equations (2.2). However, the coefficients N_1 and N_2 can be modified due to the feedback of the second harmonic on the fundamental wave. Depending on the symmetry of the tensor $(\chi^{(2)}_{\alpha\beta\gamma})$, both coefficients or only one of them may be affected. If, for example, the coupling constants $\chi^{(2)}_{\alpha\beta\gamma}$ are nonzero only if the Cartesian indices α, β, and γ are pairwise distinct, the right-hand side of Eq. (2.14) vanishes while the right-hand side of Eq. (2.15) does not. Consequently, N_2 remains unchanged, while N_1 may be modified by the quadratic nonlinearity. If N_2 is modified, it will necessarily acquire an imaginary part in our waveguide system. This is due to the fact that two counterpropagating guided waves generate bulk waves that radiate energy into the substrate and into the vacuum. In order to satisfy the boundary conditions at the surface and at the interface, the solution of Eq. (2.14) contains a component of the form $\vec{\mathcal{E}}^{(S)}\exp(iq_S z)$ in the substrate and $\vec{\mathcal{E}}^{(V)}\exp(-iq_V z)$ in the vacuum region, where $q_S=2\omega_0\sqrt{\varepsilon_L}/c$ and $q_V=2\omega_0/c$. (In the substrate far from the surface, ε_L is assumed to be independent of z.) Such a plane-wave component is not present in the solution of Eq. (2.15) unless one is in a regime where Cherenkov radiation of the second harmonic takes place. Therefore, the coefficient N_1 is normally real. The imaginary part of N_2 can be associated with the energy flux into the substrate and vacuum in the following way: We multiply Eq. (2.14) by $E_\alpha^{(0,2)*}$, sum over α, and integrate over z from $-H$ to $+H$, where $1/H$ is much smaller than the decay constants of the guided wave fields $\vec{E}^{(\pm)}$ in the vacuum and the substrate. Integrating once by parts and subtracting the conjugate complex yields the following equation:

$$-8\frac{\omega_0^2}{c^2}\int_{-H}^{H}\sum_{\alpha,\beta,\gamma}\chi^{(2)}_{\alpha\beta\gamma}E_\alpha^{(0,2)*}(z)E_\beta^{(+)}(z)E_\gamma^{(-)}(z)dz-\text{c.c.} = \sum_\alpha\left[E_\alpha^{(0,2)*}(z)\frac{\partial}{\partial z}E_\alpha^{(0,2)}(z)\right]_{-H}^{H}-\text{c.c.} \quad (2.16)$$

For H sufficiently large, the integral on the left-hand side becomes independent of H, and we may extend the integral to $\pm\infty$ to obtain finally

$$4i\frac{\omega_0^2}{c^2}\int_{-\infty}^{\infty}\sum_{\alpha,\beta,\gamma}\chi^{(2)}_{\alpha\beta\gamma}E_\alpha^{(0,2)*}(z)E_\beta^{(+)}(z)E_\gamma^{(-)}(z)dz+\text{c.c.} = -|\vec{\mathcal{E}}^{(V)}|^2 q_V-|\vec{\mathcal{E}}^{(S)}|^2 q_S. \quad (2.17)$$

The left-hand side of Eq. (2.17) is the imaginary part of the correction to the coefficient N_2 in the evolution equations due to quadratic nonlinearity. The right-hand side is obviously the energy current into the substrate and the vacuum generated by the counterpropagating guided modes $\vec{E}^{(\pm)}$. In an analogous way, it is shown that N_1 is real. The imaginary part of the coefficient N_2 gives rise to damping of nonlinear modes which depends on their amplitudes.

The two substrate materials considered in the examples of Table I, GaAs and InSb, have been treated as Kerr materials, although they also have a nonvanishing $\chi^{(2)}$. We repeat that

the experimental values of Ref. [36] for the intensity-dependent refractive index used for the data presented in Table I have to be regarded as effective Kerr coefficients which, in principle, depend on the geometry of the waveguide.

D. Resonant interaction with the second harmonic

By choosing the materials and the geometry appropriately, the dispersion curves of the guided modes in multimode systems like our example system of Fig. 1 can be arranged such that the second harmonic of a guided mode with frequency ω_0 and wave vector K is resonant (or almost resonant) with another guided mode, i.e., there is a guided mode having wave vector $\tilde{K}=2K$ and frequency $\tilde{\omega}\approx 2\omega_0$. If now a periodic grating is ruled on the surface with periodicity $a=2\pi/G$ and $K=G/2$, then a gap will open up at the frequency ω_0 in the usual way, due to the linear interaction of the mode having wave vector $K=G/2$ with the counterpropagating mode having wave vector $-G/2$ via the grating. Similarly, a frequency splitting can occur due to linear interaction between the modes with wave vector G and $-G$ (see right part of Fig. 4). If, in addition, second-order nonlinearity is present and symmetry allows for it, the mode with wave vector K interacts with the mode having wave vector $2K$ and in the same way, the mode with wave vector $-K$ interacts with the mode having wave vector $-2K$. This (quasi) resonant interaction has to be accounted for in our asymptotic procedure by including the terms

$$e^{-\tilde{\omega}t}[\nu e^{iGx}\vec{E}^{(2+)}(z)\tilde{B}_+(X,T) + \nu e^{-iGx}\vec{E}^{(2-)}(z)\tilde{B}_-(X,T)]+O(\nu^2) \tag{2.18}$$

in the expansion (2.1). $\vec{E}^{(2\pm)}(z)$ are the modal fields of the waveguide modes with wave vectors $\pm G$ and frequency $\tilde{\omega}$. Furthermore, we use the scaling $X=\nu x$ and $T=\nu t$ for the stretched coordinates and $\zeta(x)=\nu\tilde{\zeta}(x)$ for the surface profile function to ensure that the dominant effects of quadratic nonlinearity and periodic corrugation are of the same order of magnitude. Going now through the usual multiple-scale procedure, one obtains after rescaling and simple transformations of the phases

$$u_- + i\left(\frac{\partial u_+}{\partial\tau}+\frac{\partial u_+}{\partial\xi}\right)+2w_+u_+^*=0, \tag{2.19a}$$

$$u_+ + i\left(\frac{\partial u_-}{\partial\tau}-\frac{\partial u_-}{\partial\xi}\right)+2w_-u_-^*=0, \tag{2.19b}$$

$$\Lambda w_- + 2i\kappa\left(\frac{\partial w_+}{\partial\tau}+v\frac{\partial w_+}{\partial\xi}\right)+u_+^2-\mu w_+=0, \tag{2.19c}$$

$$\Lambda^* w_+ + 2i\kappa\left(\frac{\partial w_-}{\partial\tau}-v\frac{\partial w_-}{\partial\xi}\right)+u_-^2-\mu w_-=0. \tag{2.19d}$$

The functions $u_\pm(\xi,\tau)$ are related to $B_\pm(X,T)$ and $w_\pm(\xi,\tau)$ to $\tilde{B}_\pm(X,T)$. The parameters κ, μ, and v are real, while Λ is usually complex. In particular, v stands for the ratio of the group velocities of the linear waveguide modes with wave vector G and $G/2$ in the absence of periodic modulation.

Solitary wave solutions of these equations have been found by several authors [17–23] numerically and, in certain special cases, analytically. In addition to stationary solutions, even moving solitary waves have been determined [22]. The stationary ones, to which we confine our attention here, can be obtained by a reduction of Eq. (2.19) to ordinary differential equations (ODEs) via

$$u_\pm(\xi,\tau)=U_\pm(\xi)e^{i\delta\tau}, \tag{2.20a}$$

$$w_\pm(\xi,\tau)=W_\pm(\xi)e^{2i\delta\tau}, \tag{2.20b}$$

and the requirement $U_+=U_-^*=U$ and $W_+=W_-^*=W$. The resulting ODEs have the conserved quantity

$$U^2+(U^*)^2+\Lambda^*W^2+\Lambda(W^*)^2-2\delta|U|^2-2\bar{\mu}|W|^2 + 2W^*U^2+2W(U^*)^2, \tag{2.21}$$

where $\bar{\mu}=\mu+4\kappa\delta$. An example of such a stationary solitary wave is shown in Fig. 8(c). We note that in the limit $v=0$, the ODEs resulting from the reduction (2.20) can be transformed into Eqs. (11) in Ref. [37]. For these equations, analytic solutions and a detailed discussion are given there.

In the same way as the MT equations can be approximately transformed into a pair of NLS equations in the limit of weak intensities, the evolution equations (2.19) reduce to the KS equations in this limit, when the frequencies of the fundamental and the second harmonic are close to the edges of the linear gaps [18]. For example, when Λ is real and the modulus of $\Delta=(\mu-\Lambda)/(2\kappa)+2$ is much smaller than 1, one obtains [17]

$$i\frac{\partial}{\partial\tau}A-\frac{1}{2}\frac{\partial^2}{\partial\xi^2}A+2BA^*=0, \tag{2.22a}$$

$$2i\kappa\frac{\partial}{\partial\tau}B-\frac{2\kappa^2v^2}{\Lambda}\frac{\partial^2}{\partial\xi^2}B-2\kappa\Delta B+A^2=0 \tag{2.22b}$$

for the variables $A=(1/2)(u_++u_-)\exp(-i\tau)$ and $B=(1/2)(w_++w_-)\exp(-2i\tau)$.

III. STABILITY ANALYSIS

To investigate the stability of the solitary wave solutions found by solving the ordinary differential equations resulting from Eq. (2.19) via the reduction (2.20), we have carried out long-time numerical simulations by integrating the coupled evolution equations (2.19) using a split-step Fourier scheme with initial conditions corresponding to a stationary solution. The results of these simulations were not conclusive. Even when a stationary solution appeared to be quite robust against perturbations of its initial conditions on a short-time scale, it showed a sudden breakup on a long scale [>25 time units for the solution shown in Fig. 8(c)] with strong spatial fluctuations. Similar phenomena, albeit on an even longer-time scale, were observed for certain solutions of the MT equations. It was impossible to decide from the results of the

simulations whether these breakups are the result of the numerical scheme used for the integration of the partial differential equations, or whether it is the consequence of a physical instability. In order to clarify this question, we have carried out a linear stability analysis for stationary localized solutions of the four coupled equations (2.19) as well as of the MT equations. We describe this analysis in some detail for the case of Eqs. (2.19). The procedure is analogous for the MT equations. We write

$$u_{\pm}(\xi,\tau)=[U_{\pm}(\xi)+a_{\pm}(\xi,\tau)]e^{i\delta\tau}, \tag{3.1a}$$

$$w_{\pm}(\xi,\tau)=[W_{\pm}(\xi)+b_{\pm}(\xi,\tau)]e^{2i\delta\tau}, \tag{3.1b}$$

and decompose $a_{\pm}$ and $b_{\pm}$ into their real and imaginary parts, denoted by a prime and a double prime, respectively. We then linearize Eq. (2.19) with respect to the eight variables $a'_{\pm}$, $a''_{\pm}$, $b'_{\pm}$, $b''_{\pm}$. Defining the eight-component vector

$$\mathbf{p}=(a'_{+},a'_{-},b'_{+},b'_{-},a''_{+},a''_{-},b''_{+},b''_{-}) \tag{3.2}$$

one is led to the following system of linear equations:

$$\underline{\mathbf{J}}\frac{\partial}{\partial\tau}\mathbf{p}=\underline{\mathbf{M}}\mathbf{p}. \tag{3.3}$$

Here

$$\underline{\mathbf{J}}=\begin{pmatrix}\mathbf{0} & \mathbf{K}\\ -\mathbf{K} & \mathbf{0}\end{pmatrix} \tag{3.4}$$

and $\mathbf{K}$ is a diagonal 4×4 matrix with $K_{11}=K_{22}=1$ and $K_{33}=K_{44}=2\kappa$. The matrix operator $\underline{\mathbf{M}}$ has the form

$$\underline{\mathbf{M}}=\begin{pmatrix}\mathbf{H}_1 & \mathbf{A}\\ \mathbf{A}^{+} & \mathbf{H}_2\end{pmatrix}, \tag{3.5}$$

where $\mathbf{H}_1$ and $\mathbf{H}_2$ are two Hermitian operators and $\mathbf{A}$ is a matrix non-Hermitian matrix operator. Explicitly,

$$\mathbf{H}_1=\begin{pmatrix}-\delta+2W' & 1 & 2U' & 0\\ 1 & -\delta+2W' & 0 & 2U'\\ 2U' & 0 & -\overline{\mu} & \Lambda'\\ 0 & 2U' & \Lambda' & -\overline{\mu}\end{pmatrix}, \tag{3.6}$$

$$\mathbf{A}=\begin{pmatrix}-\frac{\partial}{\partial\xi}+2W'' & 0 & 2U'' & 0\\ 0 & \frac{\partial}{\partial\xi}-2W'' & 0 & -2U''\\ -2U'' & 0 & -2\kappa v\frac{\partial}{\partial\xi} & -\Lambda''\\ 0 & 2U'' & \Lambda'' & 2\kappa v\frac{\partial}{\partial\xi}\end{pmatrix}. \tag{3.7}$$

Here, a prime and a double prime denote again the real and imaginary part, respectively. The matrix $\mathbf{H}_2$ is obtained from $\mathbf{H}_1$ by changing the sign in front of W'.

With the ansatz $\mathbf{p}(\xi,\tau)=\mathbf{q}(\xi)\exp(\lambda\tau)$, Eq. (3.3) becomes a non-Hermitian eigenvalue problem $\lambda\mathbf{q}=\underline{\mathbf{L}}\mathbf{q}$, where $\underline{\mathbf{L}}=\underline{\mathbf{J}}^{-1}\underline{\mathbf{M}}$. The components of the vector $\mathbf{p}$ will from now on be regarded as complex quantities. Since $\underline{\mathbf{J}}$ and $\underline{\mathbf{M}}$ are purely real, real solutions of Eq. (3.3) are obtained from a complex one by forming linear combinations of $\mathbf{p}$ and $\mathbf{p}^*$. The structure of Eq. (3.3) is distinct from the linearizations of the nonlinear Schrödinger equation and the Karamzin-Sukhorukov equations because of the presence of the non-Hermitian operator $\mathbf{A}$. There is no reason to assume that the squares of the eigenvalues λ are real for the MT equations and the evolution equations (2.19). Therefore, the method of Pelinovsky, Buryak, and Kivshar [30] (see also [31]) for the determination of the boundary between stable and unstable regions in parameter space cannot be applied here. Within this method, the stability boundary is determined from a compatibility condition arising in an expansion in powers of the eigenvalue λ near the stability boundary. In the systems considered here, the eigenvalue associated with an instability may have a large (and unknown) imaginary part near the stability boundary.

In order to determine the spectrum of the non-Hermitian operator $\underline{\mathbf{L}}$, we discretize the spatial coordinate ξ, i.e., we work with grid points $\xi_n=n\Delta\xi$, where $n=0,\pm1,\pm2,\ldots,+N$. (In the actual calculations, the grid was shifted by $\Delta\xi/2$ for numerical convenience.)

All common numerical schemes employed for the integration of nonlinear evolution equations of the type considered here are based on a discretization of the spatial coordinate. However, there are various ways in which they deal with spatial derivatives of a function $f(\xi)$. The simplest is to replace $\partial f(\xi)/\partial\xi$ at grid point $\xi=n\Delta\xi$ by $\{f([n+1]\Delta\xi)-f([n-1]\Delta\xi)\}/(2\Delta\xi)$. We call this the derivative of type I.

Semispectral methods usually work with a regular grid, too. Their treatment of the spatial derivative corresponds to replacing $\partial f(\xi)/\partial\xi$ at grid point $\xi=n\Delta\xi$ by $-i\Sigma_{m=-N}^{N-1}D_{nm}f(m\Delta\xi)$ with

$$D_{mn}=\frac{-\pi}{N\Delta\xi}\begin{cases}1 & \text{for } m=n\\ (-1)^{m-n}\left[1-i\dfrac{\sin[\pi(m-n)/N]}{1-\cos[\pi(m-n)/N]}\right] & \text{for } m\neq n\end{cases} \tag{3.8}$$

forming a self-adjoint matrix. This way of discretizing the spatial derivative will be called the derivative of type II.

In the semispectral methods and hence in the treatment of the derivative of type II, periodic boundary conditions are implied, $f(N\Delta\xi)=f(-N\Delta\xi)$. For the derivative of type I, various boundary conditions (including periodic) can be specified. When the solitary wave solution is centered at $\xi=0$ and $N\Delta\xi$ is much larger than the spatial extent of the solitary wave, one would expect that the qualitative features of the spectrum of the discretized operator **L** are independent of the boundary conditions. This turns out to be the case for the NLS and KS equations, but not for the MT equations and Eqs. (2.19).

One consequence of discretization is the introduction of an upper bound to the continuous and purely imaginary part of the spectrum of **L** associated with scattering states. The corresponding eigenvectors are a superposition of plane waves at large distances from the solitary wave solution. In addition, the restriction to a finite domain (finite N) discretizes this part of the spectrum. We emphasize that when using the term finite spatial domain, we always mean that the boundaries of this domain are far remote from the center of the solitary wave solution such that the solitary wave field has fallen off to virtually zero at these boundaries.

We have determined the spectrum of the operator **L** after discretization for various examples and have investigated its dependence on the two parameters N and $\Delta\xi$. A typical example for the KS equations and a solitary wave solution in the unstable region of the parameter space is shown in Fig. 5. In addition to the purely imaginary part of the spectrum, there are two real eigenvalues $\lambda=\pm|\lambda|$. Their modulus is in perfect agreement with the growth rate given in Fig. 2 of Ref. [30] for this case.

Figure 6 shows the spectrum for a gap solitary wave solution of the MT equations. The symmetry of the MT equations implies that if $\lambda=\lambda'+i\lambda''$ is an eigenvalue, so are $\lambda'-i\lambda''$ and $-\lambda'\pm i\lambda''$. In addition to the purely imaginary part of the spectrum, a large number of complex eigenvalues appears, having small real parts but large imaginary parts. With increasing refinement of the discretization and increasing range $N\Delta\xi$, some of these eigenvalues move towards the imaginary axis. Most of the eigenvalues with nonzero real part are associated with eigenvectors that show rapid oscillations and normally change sign between two adjacent grid points [Fig. 7(a)]. They are sensitive to the parameter $\Delta\xi$ as well as to the way the spatial derivative is treated, and they are obviously a consequence of the discretization and correspond to numerical instabilities. They occur even in the integrable case $N_1=0$, which corresponds to the massive Thirring model. This means that numerical integration schemes can face instabilities in long-time simulations of solitary pulse propagation with the evolution equations (2.2) and (2.19) in contrast to the NLS and KS equations. They may perhaps be avoided by introducing spatial smoothing on a short length scale.

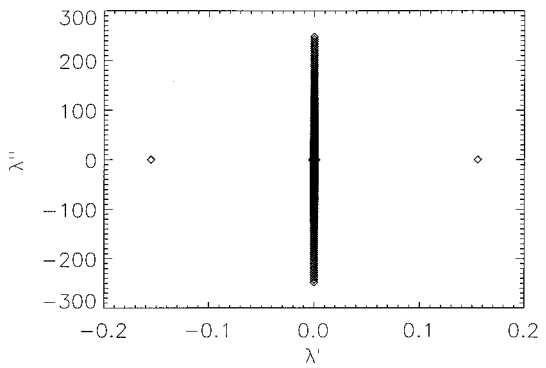

FIG. 5. Eigenvalues of the operator $\underline{\mathbf{L}}$ for a solitary wave solution of the KS equations with $\alpha=0.05$ and $\sigma=2$ (parameters defined in [30]).

Other eigenvalues with nonzero real part have eigenvectors that are largely localized at the edge of the spatial domain, i.e., they are appreciably different from zero only at $\xi\approx\pm N\Delta\xi$. They are a consequence of the finite range to which we have limited our analysis up to now.

In addition to the eigenvalues with nonzero real part that are associated with purely numerical instabilities, there can be a few that have a physical interpretation. Their associated eigenvectors vary slowly on the scale $\Delta\xi$ [Fig. 7(b)] and hence become independent of the discretization for sufficiently small $\Delta\xi$. However, for distances ξ far away from the solitary wave solution, they do not fall off to zero as in the case of the KS equations, but they are of oscillatory character. In fact, they are a superposition of generalized plane waves with complex wave numbers k that follow from the secular equation

$$|\underline{\tilde{\mathbf{L}}}(k)-\lambda\underline{\mathbf{1}}|=0, \tag{3.9}$$

where $\underline{\mathbf{1}}$ is a unit matrix and $\underline{\tilde{\mathbf{L}}}(k)$ is the matrix obtained from the operator $\underline{\mathbf{L}}$ by setting $U'=U''=W'=W''=0$ and replac-

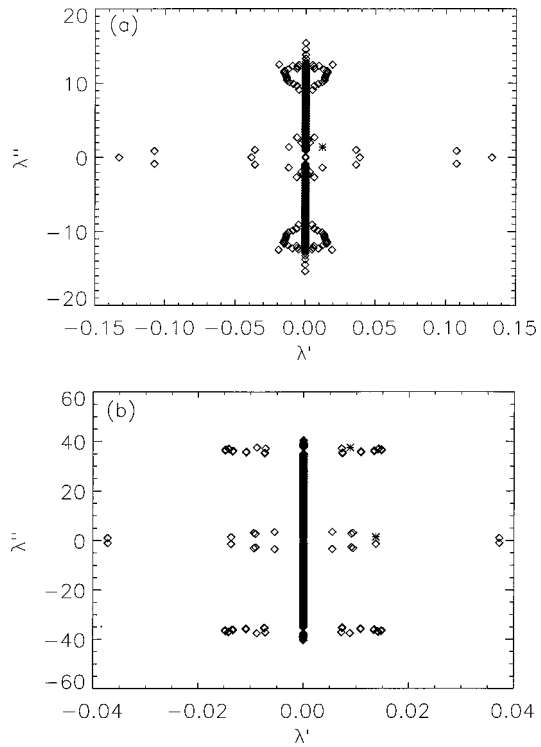

FIG. 6. Eigenvalues of the operator $\underline{\mathbf{L}}$ for a solitary wave solution of the MT equations (2.2) with parameters $N_1=3$, $N_2=1$, $\delta=-0.1$, $\Delta\xi=0.08$, $N=100$. (a) Derivative of type I; (b) derivative of type II. Eigenvector components associated with eigenvalues represented by a star are shown in Fig. 7.

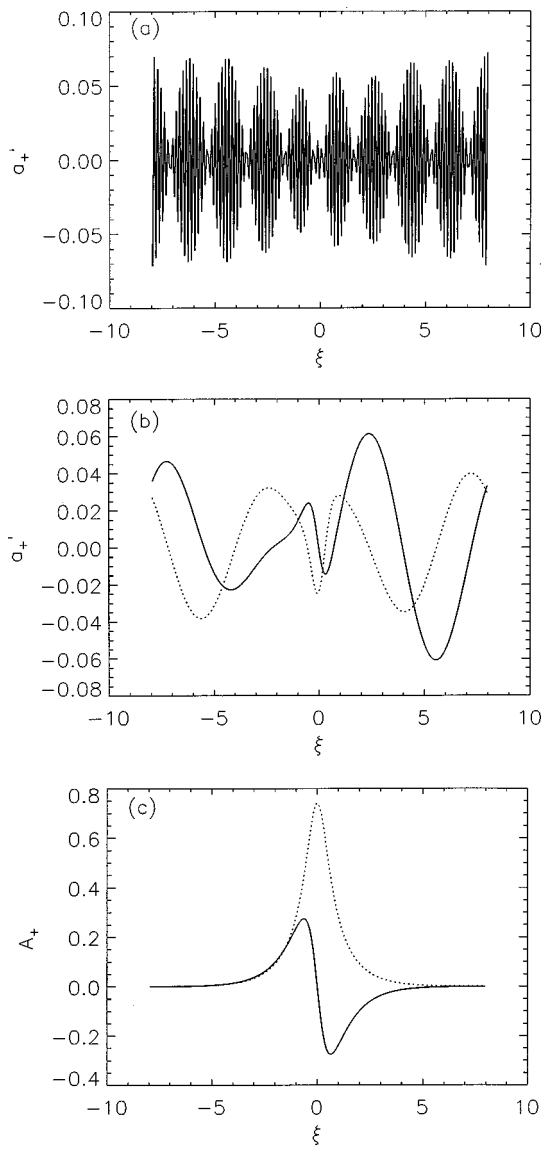

FIG. 7. Eigenvectors associated with certain eigenvalues shown in Fig. 6. (a) Real part of the components a'_+ of the eigenvector $\mathbf{q}$ corresponding to the star in Fig. 6(a). (b) Real part (solid) and imaginary part (dashed) of a'_+ associated with the lower star in Fig. 6(b) [same as star in Fig. 6(a)]. (c) Corresponding solitary wave solution having the form (2.11). Real part (solid) and imaginary part (dashed) of U are shown for comparison.

ing the derivative $\partial/\partial\xi$ by ik. [In the case of the KS and MT equations, these are 4×4 matrices while in the case of Eqs. (2.19), they are 8×8 matrices.] As the eigenvalue λ has a small real part, the wave numbers k have to be expected to have small positive as well as negative imaginary parts. The physical interpretation of these eigenmodes is the following: The solitary wave is unstable and emits radiation with frequency λ'' and (real) wave numbers k' obtained from the solutions of Eq. (3.9). In a finite spatial domain, this radiation gets reflected from the boundaries, and the reflected wave components interfere with the wave field in the neighborhood of the solitary wave solution. Similarly, in the case of periodic boundary conditions, the radiation leaving the periodicity domain on one side and reentering it on the other interferes with the wave field at the position of the solitary pulse. Therefore, the eigenvalue λ strongly depends on the boundary conditions and on the size of the spatial domain. Solitary waves that are linearly stable for a certain domain size may be unstable for another. This effect has also been observed in discrete systems [38,39]. It has to be kept in mind when interpreting the results of numerical simulations that necessarily have to be carried out on a finite domain. For parameters $N_2/N_1=2$ and $\Delta\omega=0$, an instability of the gap soliton solution of the MT equations has been found on a finite spatial domain, while this solution is predicted to be stable on an infinite domain [26].

The spectrum of the operator $\underline{\mathbf{L}}$ for solitary wave solutions of Eqs. (2.19) and the corresponding eigenvectors have structure similar to the ones discussed for the MT equations. At large distances from the solitary wave solution, the components $a_\pm$ associated with the fundamental frequency decouple from the components $b_\pm$ corresponding to the second harmonic, and the secular equation (3.9) factors. Consequently, either the components $a_\pm$ or $b_\pm$ are of nearly plane-wave character at large distances, while the other ones are localized at the solitary wave solution.

Growth rates for an infinite spatial domain may be computed generalizing a simple method that had been developed earlier for a discrete system [38]. It is based on an eigenvalue-dependent boundary condition that simulates the infinite spatial domain. We describe this approach here for Eqs. (2.19). At large distances from the solitary wave, the eigenvector $\mathbf{q}$ associated with a complex eigenvalue λ has the form

$$\mathbf{q}(\xi)=\sum_{j=1}^{4} c_j e^{ik_j(\lambda)\xi}\mathbf{w}_j(\lambda), \tag{3.10}$$

where k_j, $j=1,\ldots,4$, are the solutions of the secular equation (3.9) that correspond to exponentially decreasing partial waves in the direction away from the solitary wave, and $\mathbf{w}_j$ is the nontrivial solution of the singular linear problem

$$[\underline{\tilde{\mathbf{L}}}(k_j)-\lambda\underline{\mathbf{1}}]\mathbf{w}_j=0, \tag{3.11}$$

normalized in an appropriate way. The coefficients c_j, $j=1,\ldots,4$, are still unknown. When discretizing the spatial coordinate ξ, we use version I of the discretized derivative, replace the derivative $\partial\mathbf{q}(\xi)/\partial\xi$ at $\xi=N\Delta\xi$ by

$$\frac{1}{2\Delta\xi}\left\{\sum_{j=1}^{4}\tilde{c}_j e^{ik_j(\lambda)\Delta\xi}\mathbf{w}_j(\lambda)-\mathbf{q}([N-1]\Delta\xi)\right\}, \tag{3.12}$$

and express the coefficients $\tilde{c}_j$, $j=1,\ldots,4$, in terms of the components of the vector $\mathbf{q}(N\Delta\xi)$ through the relation

$$\mathbf{q}(N\Delta\xi)=\sum_{j=1}^{4}\tilde{c}_j\mathbf{w}_j(\lambda). \tag{3.13}$$

The four coefficients $\tilde{c}_j$ are actually overdetermined by the eight linear equations (3.13). In practice, we include in the sum on the right-hand side of Eq. (3.13) the four exponentially increasing partial waves ($j=5,\ldots,8$), invert the 8×8 matrix with column vectors $\mathbf{w}_j$, $j=1,\ldots,8$, and dis-

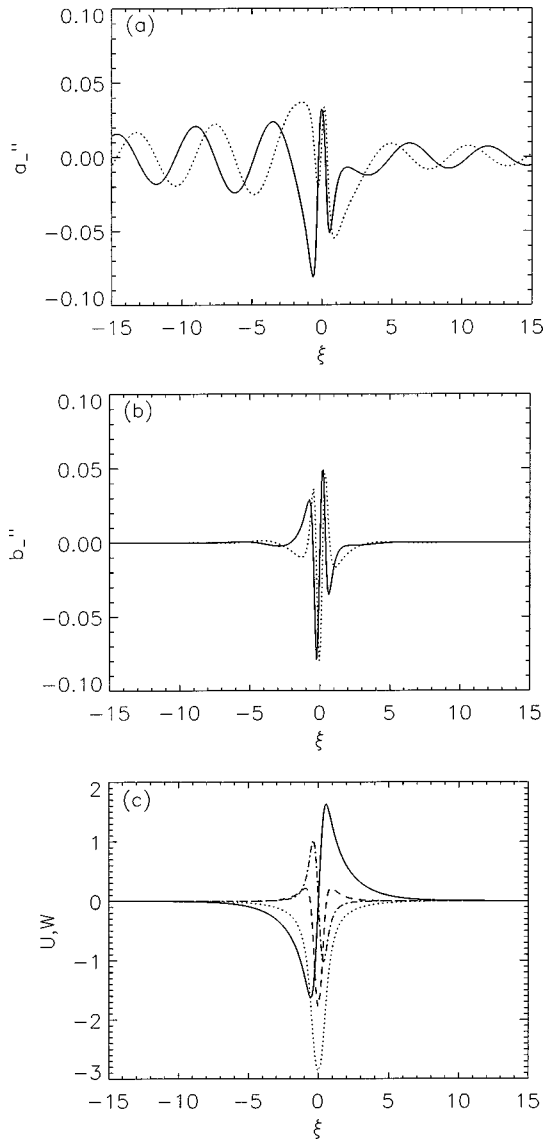

FIG. 8. Eigenvector corresponding to the eigenvalue $\lambda = 0.048 + i0.755$ for a solitary wave solution of Eqs. (2.19) having the form (2.20). Parameters: $\delta = 0.8$, $v = 0$, $\kappa = 0.5$, $\mu = 4$, $\Lambda = 1$ (infinite spatial domain). (a) Real part (solid) and imaginary part (dashed) of a''_-. (b) Real part (solid) and imaginary part (dashed) of b''_-. (c) Corresponding solitary wave solution. Solid, real part of U; dotted, imaginary part of U; dashed, real part of W; dashed-dotted, imaginary part of W.

card the coefficients $\tilde{c}_j$ with indices $j = 5, \ldots, 8$. In this way, we have eliminated $\mathbf{q}([N+1]\Delta\xi)$ in favor of $\mathbf{q}(N\Delta\xi)$. We proceed in the same way with the derivative at $\xi = -N\Delta\xi$ and are left with an eigenvalue problem of a non-Hermitian $[8(2N+1)] \times [8(2N+1)]$ matrix, which depends, however, on the eigenvalue λ via the wave numbers k_j and the vectors $\mathbf{w}_j$. Starting with an initial guess for λ and its associated eigenvector, one may use the inverse iteration scheme described in Ref. [40] with the modification that in each iteration step, the λ-dependent parts of the matrix have to be updated [38]. It has to be noted that the convergence of this procedure depends on the initial guess for the eigenvalue and eigenvector and cannot always be achieved.

Figure 8 shows the resulting eigenvector for the eigenvalue $\lambda \approx 0.048 + i0.755$ corresponding to an instability of a solitary wave solution with profile also displayed in Fig. 8. While the components $b_\pm$ associated with the second harmonic are localized in the region of the solitary wave, the components $a_\pm$ are spatially extended and decay slowly with increasing distance from the solitary wave. Making use of the smallness of the growth rate λ' in comparison to $|\lambda''|$, we may expand

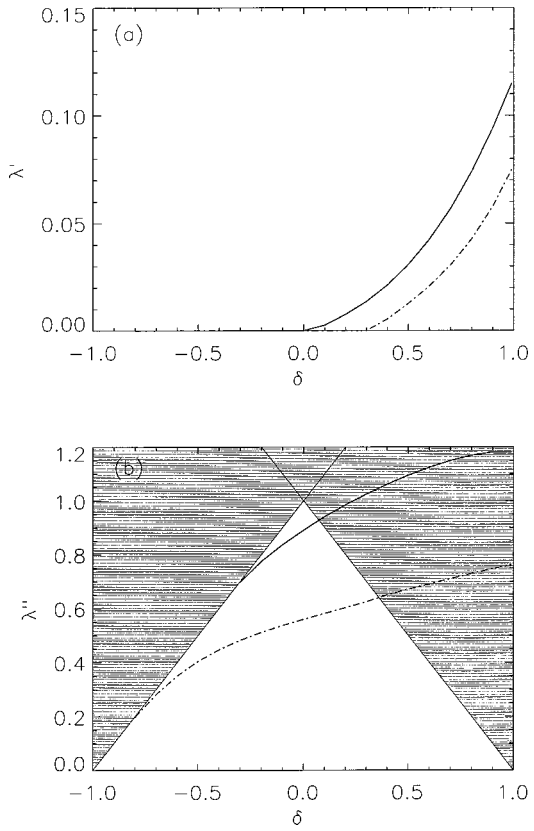

FIG. 9. Dependence on frequency of two eigenvalues of the operator $\mathbf{L}$ for stationary solitary wave solutions of Eqs. (2.19) in an infinite spatial domain. Parameters: $v = 0$, $\kappa = 0.5$, $\mu = 4$, $\Lambda = 1$. Gray: radiative regime.

$$k_j(\lambda' + i\lambda'') = -\kappa_j(\lambda'') + i\lambda' s_j(\lambda'') + O((\lambda')^2) \tag{3.14}$$

with real wave numbers κ_j and real inverse group velocities s_j. The perturbation $\mathbf{p}(\xi, \tau)$ at large distances from the solitary wave may then be written in the following approximate form:

$$\mathbf{p}(\xi, \tau) \approx \sum_j c_j e^{\lambda'(\tau - s_j\xi)} e^{-i(\kappa_j\xi - \lambda''\tau)} \mathbf{w}_j, \tag{3.15}$$

which supports the interpretation of the solitary wave radiating plane waves having envelopes that move with the group velocities s_j^{-1}.

In Fig. 9, the dependence of two eigenvalues λ on the frequency of the gap solitary wave solutions is shown. The parameters in Eqs. (2.19) have been chosen to be the same as for the solution shown in Fig. 8(c). By letting δ vary between 1 and -1, we sweep the frequency of the fundamental component of the solitary wave through the gap. With decreasing

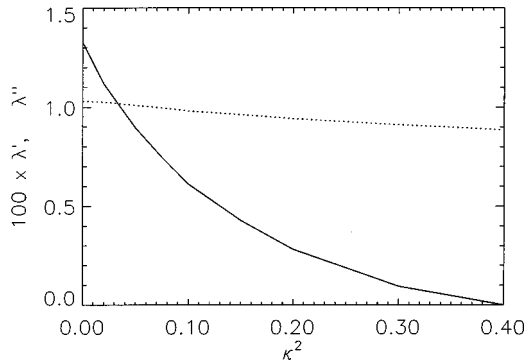

FIG. 10. Dependence of the eigenvalue λ on the diffusion length κ for stationary solitary wave solutions (2.11) of Eq. (2.10) with $\delta=-0.1$; solid, real part; dotted, imaginary part.

δ, the growth rates λ' diminish. Shortly after a curve λ'' versus δ enters the white triangle from the right in Fig. 9(b), the corresponding growth rate λ' becomes zero. Within this white triangle, the frequency $\delta\pm\lambda''$ of the perturbation $a_{\pm}(\xi,\tau)e^{i\delta\tau}$ of the solitary wave's fundamental component is in the gap of the fundamental mode and consequently, $\mathbf{q}(\xi)$ decays exponentially away from the solitary wave solution even if $\lambda'=0$. On the left side of the value of δ at which λ' has become zero, λ'' is the relative frequency of an internal mode of the solitary wave solution. This scenario is very similar to the one found by Barashenkov *et al.* for the MT equations [26]. The two λ'' versus δ curves of Fig. 9(b) terminate at the left boundary between the white triangle and the radiative regime. Beyond this boundary, there may be resonances in the continuous spectrum of the operator $\underline{\mathbf{L}}$ which would form a continuation of these two discrete branches of eigenvalues. For $\delta<0$, no instabilities have been found of the solitary wave solution of Eq. (2.19) with parameters $v=0$, $\kappa=0.5$, $\mu=4$, $\Lambda=1$. Although our search procedure does not guarantee finding all possible instabilities, there is a high probability that the center of the gap ($\delta=0$) is a boundary of stability for this set of parameters.

In the same way, this type of instability on an infinite spatial domain has been investigated for the MT equations (2.2). Its occurrence for $N_1\neq 0$ and sufficiently negative values of δ have been predicted by Barashenkov *et al.* [26]. For example, in the case $N_1=N_2=1$ and $\delta=-0.1$, an unstable mode exists with eigenvalue $\lambda\approx 0.013+i1.0$. The MT equations (2.2) with $N_1=N_2$ are obtained from the evolution equations (2.10) in the limit of vanishing diffusion length κ. The growth rate λ' has been found to decrease rapidly with increasing κ reaching zero at $\kappa\approx 0.4$ (Fig. 10). This suggests that a finite diffusion length κ seems to have a stabilizing effect on the gap solitary solutions.

In a very recent work [41], Champneys *et al.* searched for solitary wave solutions of Eqs. (2.2) with additional dispersion terms $D\partial^2 A_+/\partial\xi^2$ in Eq. (2.2a) and $D\partial^2 A_-/\partial\xi^2$ in Eq. (2.2b). They call the solitary wave solutions of the MT equations (2.2) ''structurally unstable,'' because they found that no branch of solitary wave solutions of the extended evolution equations approaches the MT solutions in the limit $D\rightarrow 0$. However, it has to be noted that addition of the above dispersion terms removes the gap in the linear dispersion relation. Consequently, solitary wave solutions of these extended equations have an exceptional character comparable to intrinsic localized in-band modes in discrete lattices and generalized nonlinear Schrödinger equations [42,43].

IV. CONCLUSIONS

In summary, stationary gap solitary waves have been discussed as solutions of evolution equations derived for example Bragg gratings in the form of slab waveguides with a periodically corrugated surface. Plasmon polaritons propagating in a metal film on a nonlinear dielectric substrate were considered as well as SOI structures. The evolution equations contain third-order nonlinearity (conventional ''gap solitons''), nonlinearity due to coupling of the electromagnetic field to a diffusion equation, which may be considered as a simple model for the SOI structures and which gives rise to an effective nonlocal third-order nonlinearity, nonresonant second-order nonlinearity, which gives rise to an effective third-order nonlinearity with a complex nonlinear coupling coefficient, and resonant coupling to the second harmonic via second-order nonlinearity. The stability of solitary solutions of these equations has been investigated via a numerical linear stability analysis. Confirming analytic work on the stability of MT solitons [26], it reveals an instability associated with a complex growth rate with small real part. This has important implications for numerical simulations as this growth rate is sensitive to the boundary conditions at the edges of the spatial domain. This type of instability has been encountered earlier in various continuous (e.g., [44–47]) as well as discrete [38] systems. Also, numerical instabilities arise in such simulations that cannot occur in systems like the nonlinear Schrödinger and Karamzin-Sukhorukov equations.

ACKNOWLEDGMENTS

We would like to thank D. Pelinovsky for sending us results prior to publication, D. Bonart for helpful discussions, I. Barashenkov for a helpful remark on the manuscript, and Yu. Kivshar for a useful comment. Financial support from the Deutsche Forschungsgemeinschaft (Graduiertenkolleg Komplexität in Festkörpern: Phononen, Elektronen und Strukturen, and Grant No. Ma 1074/6) is gratefully acknowledged.

[1] Wei Chen and D. L. Mills, Phys. Rev. Lett. **58**, 160 (1987).
[2] D. L. Mills and S. E. Trullinger, Phys. Rev. B **36**, 947 (1987).
[3] J. E. Sipe and H. G. Winful, Opt. Lett. **13**, 132 (1988).
[4] C. M. de Sterke and J. E. Sipe, Phys. Rev. A **38**, 5149 (1988).
[5] D. N. Christodoulides and R. I. Joseph, Phys. Rev. Lett. **62**, 1746 (1989).
[6] A. B. Aceves and S. Wabnitz, Phys. Lett. A **141**, 37 (1989).
[7] J. M. Bilbaud, C. T. Kamga, and M. Remoissenet, in *Nonlin-*

ear Coherent Structures in Physics and Biology, edited by M. Remoissenet and M. Peyrard (Springer, Berlin, 1991), p. 195.
[8] G. P. Agrawal, in *Contemporary Nonlinear Optics*, edited by G. P. Agrawal and R. W. Boyd (Academic Press, Boston, 1992), p. 41.
[9] B. J. Eggleton, R. E. Slusher, C. M. de Sterke, P. A. Krug, and J. E. Sipe, Phys. Rev. Lett. **76**, 1627 (1996).
[10] N. D. Sankey, D. F. Prelewitz, and T. G. Brown, Appl. Phys. Lett. **60**, 1427 (1992).
[11] N. D. Sankey, D. F. Prelewitz, T. G. Brown, and R. C. Tiberio, J. Appl. Phys. **73**, 7111 (1993).
[12] D. F. Prelewitz and T. G. Brown, J. Opt. Soc. Am. B **11**, 304 (1994).
[13] A. Lietoila and J. F. Gibbons, Appl. Phys. Lett. **40**, 624 (1982).
[14] D. Agassi, J. Appl. Phys. **55**, 4376 (1984).
[15] Yu. S. Kivshar, Phys. Rev. B **51**, 1613 (1995).
[16] Yu. S. Kivshar, O. A. Chubykalo, O. V. Usatenko, and D. V. Grinyoff, Int. J. Mod. Phys. B **9**, 875 (1995).
[17] R. Scheibenzuber, A. P. Mayer, and A. A. Maradudin, Verh. Dtsch. Phys. Ges. IV **31**, 1343 (1996).
[18] C. Conti, S. Trillo, and G. Assanto, Phys. Rev. Lett. **78**, 2341 (1997).
[19] C. Conti, S. Trillo, and G. Assanto, Opt. Lett. **22**, 445 (1997).
[20] H. He and P. D. Drummond, Phys. Rev. Lett. **78**, 4311 (1997).
[21] C. Conti, G. Assanto, and S. Trillo, Opt. Lett. **22**, 1350 (1997).
[22] T. Peschel, U. Peschel, F. Lederer, and B. A. Malomed, Phys. Rev. E **55**, 4730 (1997).
[23] C. Conti, S. Trillo, and G. Assanto, Phys. Rev. E **57**, R1251 (1998).
[24] Yu. N. Karamzin and A. P. Sukhorukov, Pis'ma Zh. Éksp. Teor. Fiz. **20**, 734 (1974) [JETP Lett. **20**, 339 (1974)].
[25] M. Picciau, G. Leo, and G. Assanto, J. Opt. Soc. Am. B **13**, 661 (1996).
[26] I. V. Barashenkov, D. E. Pelinovsky, and E. V. Zemlyanaya, Phys. Rev. Lett. **80**, 5117 (1998).
[27] W. E. Thirring, Ann. Phys. (N.Y.) **3**, 91 (1958).
[28] E. A. Kuznetsov and A. V. Mikhailov, Teor. Mat. Fiz. **30**, 303 (1977) [Theor. Math. Phys. **30**, 193 (1977)]; D. J. Kaup and A. C. Newell, Lett. Nuovo Cimento **20**, 325 (1977).
[29] V. E. Zakharov and A. B. Shabat, Zh. Éksp. Teor. Fiz. **61**, 118 (1971) [Sov. Phys. JETP **34**, 62 (1972)].
[30] D. E. Pelinovsky, A. V. Buryak, and Yu. S. Kivshar, Phys. Rev. Lett. **75**, 591 (1995).
[31] I. V. Barashenkov, Phys. Rev. Lett. **77**, 1193 (1996).
[32] A. P. Mayer, A. A. Maradudin, R. Garcia-Molina, and A. D. Boardman, Opt. Commun. **72**, 244 (1989).
[33] G. K. Newboult, D. F. Parker, and T. R. Faulkner, J. Math. Phys. **30**, 930 (1989).
[34] R. Scheibenzuber, Staatsexamensarbeit, University of Regensburg, 1996; R. Scheibenzuber, A. P. Mayer, and A. A. Maradudin (unpublished).
[35] H. Raether, *Excitations of Plasmons and Interband Transitions by Electrons*, Springer Tracts in Modern Physics Vol. 88 (Springer, Berlin, 1980).
[36] G. I. Stegeman, IEEE J. Quantum Electron. **QE-18**, 1610 (1982).
[37] A. S. Kovalev, K. V. Kladko, and O. V. Usatenko, J. Phys. Soc. Jpn. **64**, 2455 (1995).
[38] D. Bonart, A. P. Mayer, and U. Schröder, Phys. Rev. B **51**, 13 739 (1995).
[39] J. N. Teixeira Rabelo and A. A. Maradudin, Phys. Lett. A **205**, 349 (1995).
[40] W. H. Press, B. P. Flannery, S. A Teukolsky, and W. T. Vetterling, *Numerical Recipes* (Cambridge University Press, Cambridge, England, 1986).
[41] A. R. Champneys, B. A. Malomed, and M. J. Friedman, Phys. Rev. Lett. **80**, 4169 (1998).
[42] D. Bonart, Phys. Lett. A **233**, 233 (1997).
[43] J. Fujioka and A. Espinosa, J. Phys. Soc. Jpn. **66**, 2601 (1997).
[44] I. V. Barashenkov, M. M. Bogdan, and T. Zhanlav, in *Nonlinear World: IV International Workshop on Nonlinear and Turbulent Processes in Physics, Kiev, 1989*, edited by V. G. Bar'yakhtar *et al.* (World Scientific, Singapore, 1990), Vol. 1, p. 3.
[45] I. V. Barashenkov, M. M. Bogdan, and V. I. Korobov, Europhys. Lett. **15**, 113 (1991).
[46] H. T. Tran, J. D. Mitchell, N. N. Akhmediev, and A. Ankiewicz, Opt. Commun. **93**, 227 (1992).
[47] R. L. Pego, P. Smereka, and M. I . Weinstein, Nonlinearity **8**, 921 (1995).